environments

MDPI

Article

Structural Assessment of Reinforced Concrete Beams Incorporating Waste Plastic Straws

Jamal M. Khatib [1,*], Ali Jahami [1], Adel Elkordi [1], Hakim Abdelgader [2,3] and Mohammed Sonebi [4]

1 Faculty of Engineering, Beirut Arab University, Beirut 11 5020, Lebanon; a.jahmi@bau.edu.lb (A.J.); a.elkordi@bau.edu.lb (A.E.)
2 Department of Civil Engineering, University of Tripoli, Tripoli 83038, Libya; h.abdelgader@uot.edu.ly
3 Faculty of Civil and Environmental Engineering, Gdansk University of Technology, Ul. Bbriela Narutowisza 11/12, 80-233 Gdansk, Poland
4 School of Natural and Built Environment, Queens University of Belfast, Belfast BT9 5AG, UK; m.sonebi@qub.ac.uk
* Correspondence: j.khatib@bau.edu.lb or j.m.khatib@wlv.ac.uk

Received: 20 August 2020; Accepted: 26 October 2020; Published: 29 October 2020

Abstract: The behavior of reinforced concrete beams containing fibers made of waste plastic straws (WPSs) under the three point bending test is examined. The effect of WPS fiber addition on the compressive and split tensile strength is reported. Four concrete mixes were prepared. The control mix PS-0 had a proportion of 1 cement: 1 sand: 2 coarse aggregate and a water cement ratio of 0.4. In the other three mixes PS-0.5, PS-1.5 and PS-3, 0%, 0.5%, 1.5% and 3% of WPS fiber (by volume) was added respectively. The results show that at 0.5% WPS, there is slight increase in compressive strength. However, beyond 0.5% addition, a decrease in compressive strength is observed. The split tensile strength shows a systematic increase with the addition of WPS fibers. The reinforced concrete beams containing WPS fibers show higher ductility as demonstrated by the larger ultimate tensile strain and ductility index (Δ_u/Δ_y). There is a tendency to have more fine cracks with the presence of WPS fibers.

Keywords: waste plastic straws; load; deflection; strain measurements; concrete damage; ductility

1. Introduction

Concrete is an essential material in construction and consumes large amounts of natural resources. Replacing these resources with recycled or waste product would be advantageous to the economy and the environment. Different types of waste plastic, for example, are generated daily and the majority is disposed of in open spaces and landfill sites. Concrete has the ability to incorporate waste materials including waste plastic.

Concrete has numerous beneficial properties, for example, great compressive strength, toughness and other durability properties. However, concrete is a brittle material and its tensile strength is low. Adding fibers can overcome these weaknesses and produce concrete that is more ductile has cracks with reduced width. Reducing crack width would reduce the ingress of aggressive species into concrete, thus enhancing its durability. Different types of fibers can be added to the concrete mix including; asbestos, rubber, glass, plastic and bamboo fibers [1–8]. Plastic fibers can be produced from unused and recycled plastic.

Perumelsamy et al. [9] studied the effect of adding up to 3% glass fiber on concrete properties. While there is slight reduction in workability in the presence of fibers, however, an improvement in flexural and split tensile strength is observed. Similar results were obtained elsewhere [10,11].

Vikrants et al. [12] investigated the effect of adding steel fiber on the performance of concrete. They found that the inclusion of steel fibers in concrete improve the compressive strength, split tensile strength and flexural strength. An increase of 55% in flexural strength was observed in the presence of fibers.

Yakhlaf [13] studied the properties of concrete containing carbon fibers and found that the compressive strength, split tensile strength and flexural strength are enhanced in the presence of fibers. Similar results were obtained on concrete and mortar incorporating carbon fibers [14,15].

Phong [16] examined the use of bamboo fibers in concrete. An increase in fiber content up to 1.0% led to an increase in compressive strength, ductility, toughness and tensile strength. However, the workability of concrete was found to decrease with the increase in fiber content.

Bae [17] reported the findings on concrete containing recycled polyethylene terephthalate (PET) fiber. The fiber contents were 0.5%, 0.75% and 1.0% of concrete volume. They showed that both elastic modulus and compressive strength decreased as fiber content increased. The drying shrinkage slowed down and ductility increased in the presence of PET. Similar results were obtained elsewhere [18–20].

Wang et al. [21] studied the mechanical and durability performance of combined macro polypropylene (PP) fiber and rubberized concrete. Two rubber volume contents were considered: 10% and 15% incorporating with fiber volume fraction of 0.5%. Fracture energy, compressive strength, ultrasonic pulse velocity (UPV) and shrinkage were considered in this study. Results showed that the fracture energy of plain concrete was enhanced by adding PP fiber and rubberized concrete. As for compressive strength and UPV, they showed a good quality of concrete. Durability results showed an enhancement in fiber concrete samples compared to plain concrete samples. Similar studies were conducted on synthetic fibers [22,23]. This wider aim of this research is to study the effect of adding waste plastic straw (WPS) fibers on the structural performance of reinforced concrete beams. Future research will attempt to examine the effect this type of fibers on the behavior of reinforced concrete beams and slabs when subjected to dynamic and impact loads [24–29].

2. Materials and Methods

2.1. Materials

The cement used was CEM 1 according to ASTM C192 [30]. The coarse aggregates used consisted of a 10 mm crushed limestone with a density of 2550 kg /m^3, whereas the fine aggregate used consisted of a 5 mm sand, having a density of 2650 kg/m^3. The waste plastic straws (WPSs) were obtained from a local restaurant. They were shredded and cut to 2 mm in width and 30 mm in length as shown in Figure 1. The chemical admixtures used were a ViscoCrete, which is a modified polycarboxylates and conforms to BS EN 934-2 [31]. The properties of the ViscoCrete are shown in Table 1.

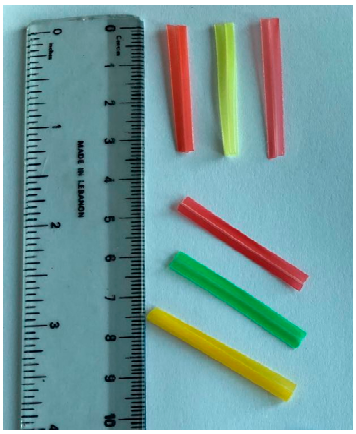

Figure 1. Shredded waste plastic straws (WPSs).

Table 1. Properties of the admixture used in the concrete mix.

Color	Storage Temperature	Chemical Base	Density	PH Value	Quantity	Mixing Time
Yellowish liquid	+5 °C to +35 °C	Synthetic Poly Carboxylates Ethers	1.05 Kg/L	4.3 + 0.5	0.6–2% of the weight of cement	60 s

2.2. Mix Design

Based on a series of trial mixes, a concrete mix having a proportion of 1 (cement): 1 (fine aggregate): 2 (coarse aggregate) by weight was selected as the control mix (PS-0) with no waste plastic straw fibers. The water to cement ratio was 0.4. In the other mixes (PS-0.5, PS-1 and PS-3), 0.5%, 1.5% and 3% of WPS fibers was added respectively. These percentages were based on a previous study conducted on plastic straw fibers [32]. Details of all concrete mixes are presented in Table 2.

Table 2. Details of concrete mixes.

	Weight (kg/m^3)					
Mix	**Cement**	**Sand**	**Water**	**Gravel**	**WPS ***	**Admixture ****
PS-0	670	670	270	1340	0	0
PS-0.5	670	670	270	1340	0.5	0.1
PS-1.5	670	670	270	1340	1.5	0.15
PS-3	670	670	270	1340	3	0.2

* % of waste plastic straws (WPS) by volume of concrete. ** By weight of cement (kg).

2.3. Mixing Procedure

The dry materials required for each mix were weighed. The coarse aggregates were placed in the mixer first followed by the fine aggregate, cement and fibers. They were then mixed for 2 min. The water and chemical admixture were then the added to the dry materials and mixing continued until proper mixing (Figure 2). This normally took about 3 min. After mixing, the slump test was conducted for all mixes. The slump values were 53, 47, 15 and 7 mm for mixes with 0%, 0.5%, 1.5% and 3% WPS respectively. Specimens were then cast in their molds (Figure 3). For each mix, six (10 cm diameter and 20 cm length) cylindrical specimens, three (10 cm × 10 cm × 10 cm) cubic specimens, and one (20 cm × 30 cm × 150 cm) beam were cast. After casting, the cubes and cylinders were then placed in water at 20 °C until the time of testing. However, the beam was covered with wet hessian and plastic sheeting. The hessian was kept moist throughout the curing period. All specimens were tested at 28 days.

Figure 2. Concrete mixer.

Figure 3. Casting and compacting.

2.4. Beam Details

The longitudinal and cross section of the reinforced concrete beam are shown in Figures 4 and 5 respectively. Each beam was reinforced with three 10 mm diameter rebars at the bottom, and two 6 mm diameter rebars at the top. As for the shear reinforcement, an 8 mm diameter closed stirrups were placed at a spacing of 10 cm. The yield and ultimate strength for the steel rebars were 420 MPa and 580 MPa respectively.

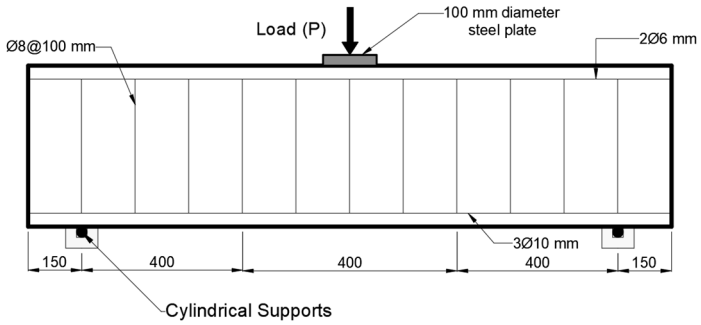

Figure 4. Longitudinal section of the beam (mm).

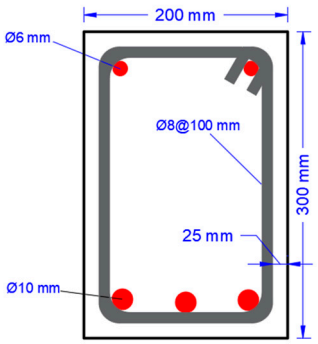

Figure 5. Beam cross section (mm).

2.5. Testing

2.5.1. Compressive Strength

The cubes were used to conduct the compressive strength test according to ASTM C39 [33].

2.5.2. Split tensile Strength

The cylinders were used to conduct the split tensile strength according to ASTM C496 [34].

2.5.3. Beam Testing

Beams were tested using the three-point bending test as shown in Figure 4. The test was conducted according to (ASTM D790-03, ASTM C78 and ASTM C1609/C1609M-19) [35–37], where the beam was loaded at midspan as shown in Figure 4. The load was applied at 5 KN increment until yield and then the load continued until failure.

Strain measurement was conducted according to (ASTM E606/E606M-12) [38], using steel demec points that were fixed to the beam at specific distances as shown in Figure 6. A mechanical strain gauge (Figure 7) was used according to (ASTM E251-92) [39] to measure the strain in the beam after subjecting it to increasing point load by the "D7940" testing machine.

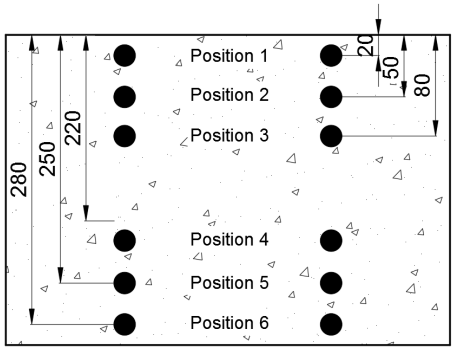

Figure 6. Demec points location (mm).

Figure 7. Mechanical strain gauge.

2.6. Numerical Modeling

Beside the experimental work, the beams were modeled numerically. The commercial software ABAQUS was used for this purpose. The concrete body was modeled as "C3D8R" an 8-node linear brick element, whereas the steel rebars were modeled as "T3D2" a 2-node linear 3-D truss element. As for the supports, they were modeled as rigid elements since their distortions are negligible compared to the concrete beam. Figure 8 shows all model details for the modeled concrete beams.

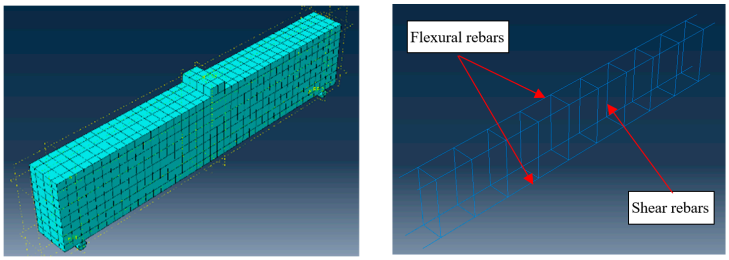

Figure 8. Numerical modeling for concrete beams.

Regarding material properties, the concrete material was defined using the "CDP" concrete damage plasticity method. This method considers the full nonlinear behavior of concrete as shown in Figure 9. Whereas the steel rebar material was defined as the elastic-perfectly plastic material, which consider the elastic response of steel until reaching the yielding limit where it turns into a perfect plastic material as shown in Figure 10.

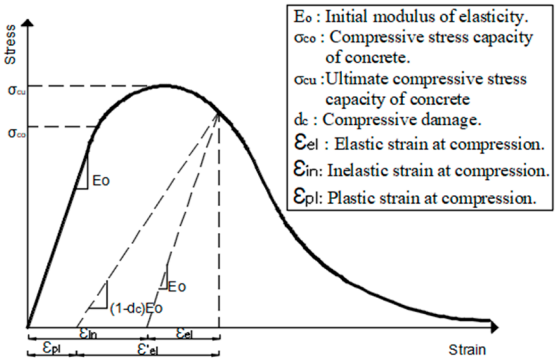

Figure 9. Concrete damage plasticity (CDP) model for concrete.

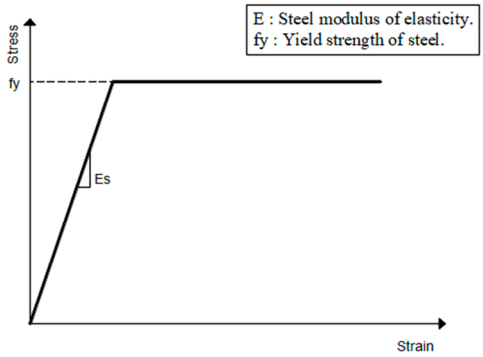

Figure 10. Elastic-perfectly plastic behavior of steel.

In the case of concrete containing WPS fibers, stress–strain curves where updated based on the compressive strength, split tensile strength and elasticity modulus. Both the compressive and split tensile strength were determined experimentally, while the elasticity modulus E_c in MPa was determined using the following ACI318-14 [40] equation:

$$E_c = 0.043 {w_c}^{1.5} \sqrt{f'_c} \quad (1)$$

where, w_c is concrete density (kg/m^3) and f'_c is the compressive strength (MPa).

3. Results and Discussion

3.1. Experimental Results

The results showed a slight increase (around 3.3%) in the compressive strength for concrete containing 0.5% WPS (PS-0.5) compared to the control specimen (PS-0; Figure 11). Beyond this specimen, the compressive strength showed to be decreased when increasing the percentage of WPS. For example, the compressive strength for specimens PS-1.5 and PS-3 was 36.5 MPa and 35.9 MPa respectively. As for the split tensile strength, results showed that increasing the percentage of plastic straws helped in increasing the split tensile strength of the specimens as shown in Figure 12. The split tensile strength was increased from 4.19 MPa for specimen PS-0 to 4.47 MPa for specimen PS-3 with an increasing percentage of 6.7%. This increase affected the ratio between tension to compression

strength (f_t/f_c) of a specimen. This is clarified in Table 3, where this ratio was increased from 10.8% for specimen PT-0 to 12.5% for specimen PT-3.

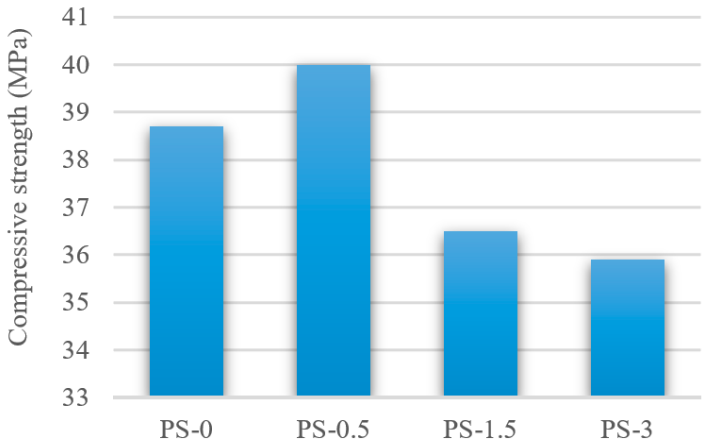

Figure 11. Compressive strength for concrete mixes.

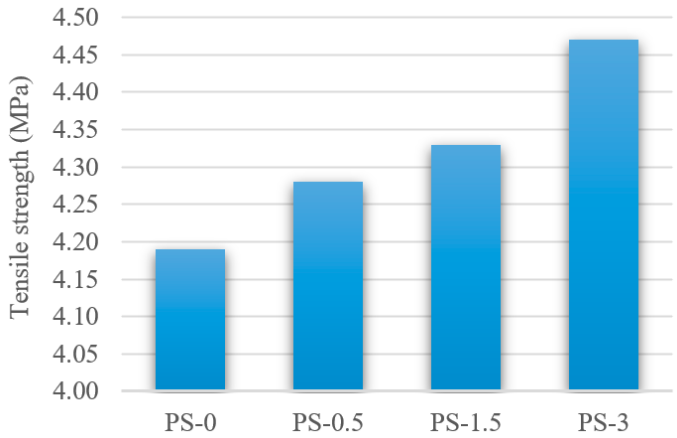

Figure 12. Split tensile strength for concrete mixes.

Table 3. Compressive and split tensile strength of tested specimens.

Sample	"f_c" Compressive Strength(MPa)	"f_t" Split Tensile Strength (MPa)	f_t/f_c
PS-0	38.70	4.19	0.108
PS-0.5	40.00	4.28	0.107
PS-1.5	36.50	4.33	0.119
PS-3	35.90	4.47	0.125

Three-point bending test results showed a higher ductility for the beams containing WPS fibers. In order to measure the ductility of the beams, the ductility factor was introduced in Table 4, which is the ratio between the deflection at the yield point and the deflection at failure. The ductility ratio increased from 3.7 for the control beam (PS-0) to 8 for beam incorporating 3% WPS (PS-3), which is an increase of 113%. This may be due to the higher tensile strength for the concrete containing WPS fibers as shown previously in Figure 12. Figure 13 shows the full load-deflection curve for beams containing 0%, 0.5%, 1.0% and 3% WPS fiber respectively. According to these figures, it can be seen that the beam with 0.5% of WPS fibers (PS-0.5) showed a higher load and deflection than the control beam (PS-0). The failure load for beams PS-0.5 was 192.7 kN compared with 181.4 kN for the control beam PS-0. However, beams containing 1.5% and 3% WPS showed similar failure load to that of the control beam, which is similar to the compression test results shown previously in Figure 11.

Table 4. Three-point bending test results.

Beam	Maximum Load "P_{max}" (kN)	$P_{max(PS)}/P_{max(0)}$	Δ_u (mm)	Δ_y (mm)	Δ_u/Δ_y
PS-0	181.4	—	15.5	4.2	3.7
PS-0.5	192.7	1.062	25.5	4.2	6.1
PS-1.5	182.7	1.007	29.0	4.6	6.3
PS-3.0	181.3	0.999	38.4	4.8	8.0

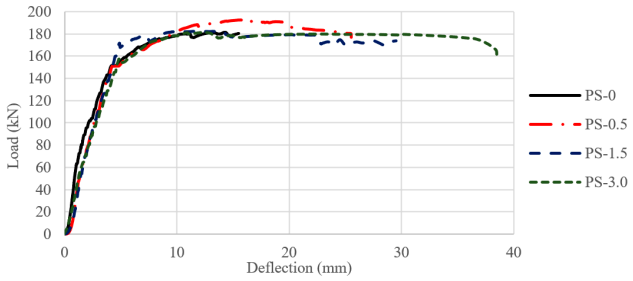

Figure 13. Load–deflection curve for all beams.

Figures 14–17 shows the strain measurements for beams containing 0%, 0.5%, 1.0% and 3% WPS fiber respectively. As the load increased, the strain at the top and bottom increased. Additionally, as the percentage of WPS increases, the strain at the same load level increased. For instance, the maximum tensile strain (bottom) for beam PS-0 at 128 kN loading was 0.0012, whereas for beam PS-3 was 0.0024. The same trend was observed for the compressive strain (top) where the strain value was 0.00057 for beam PS-0 and 0.00059 for beam PS-3. Moreover, as the load increased, the neutral axis depth decreased as shown in Table 5. The presence of fibers caused a decrease in neutral axis depth at the same applied load. At P = 128 kN, the depth of the neutral axis was 10.5 mm, 9.8 mm, 7.9 mm and 7.4 for beams PS-0, PS-0.5, PS-1.5 and PS-3.0 respectively. This indicates that the decrease in the neutral axis depth between Beams PS-0 and PS-3.0 was 30%.

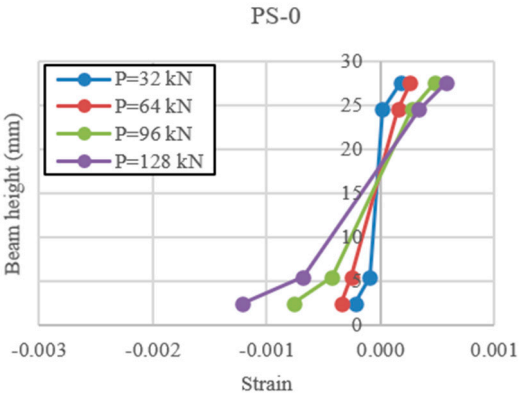

Figure 14. Strain diagram for beam PS-0.

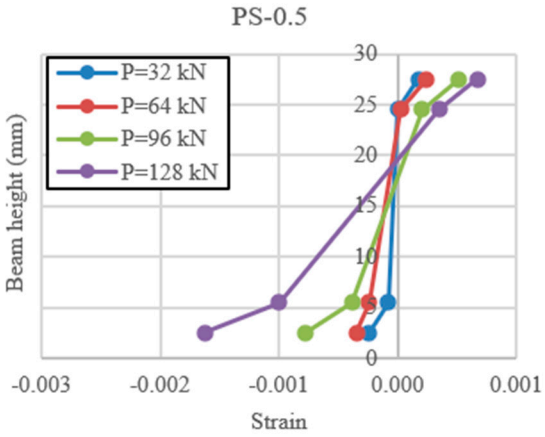

Figure 15. Strain diagram for beam PS-0.5.

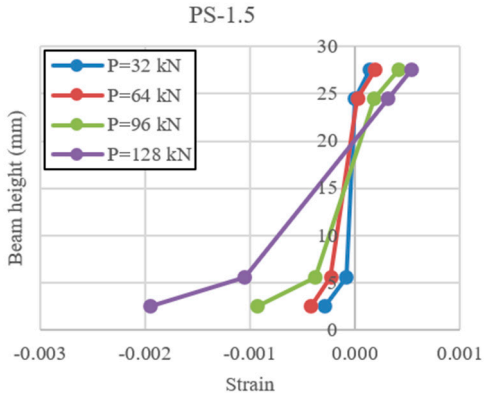

Figure 16. Strain diagram for beam PS-1.5.

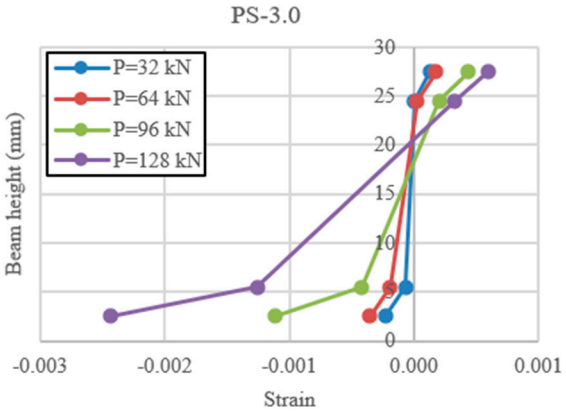

Figure 17. Strain diagram for beam PS-3.

Table 5. Neutral axis depth for all beams.

PS-0		PS-0.5		PS-1.5		PS-3	
P (kN)	**x (mm)**	**P (kN)**	**x (mm)**	**P (kN)**	**x (mm)**	**P (kN)**	**x (mm)**
32	13.6	32	13.2	32	11.5	32	10.8
64	13.3	64	12.9	64	10.9	64	10.5
96	12.1	96	12.5	96	10.2	96	9.5
128	10.5	128	9.8	128	7.9	128	7.4

Figures 18–21 show the failure patterns for beams containing 0%, 0.5%, 1.0% and 3% WPS fiber respectively. It can be observed that the mode of failure for all beams was mainly in flexure. The main cracks took place around the middle of the beams and tended to be vertical. Diagonal cracks were also observed towards the end of the test. However, these cracks tend to be finer than the main vertical cracks. Cracks started from the bottom face of the beams and extended towards the top face as the load increased. As the percentage of WPS fibers increased the beam mid-span deflection increased due to the higher ductility, which led to a higher mid span deflection as can be seen in Figure 21 for beam PS-3 compared to beam PS-0 (Figure 18).

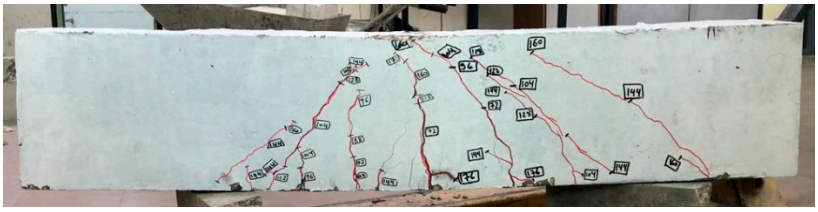

Figure 18. Crack pattern for beam PS-0.

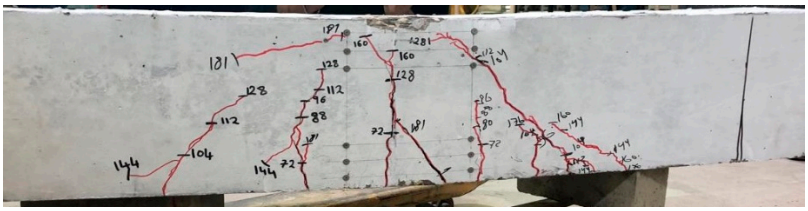

Figure 19. Crack pattern for beam PS-0.5.

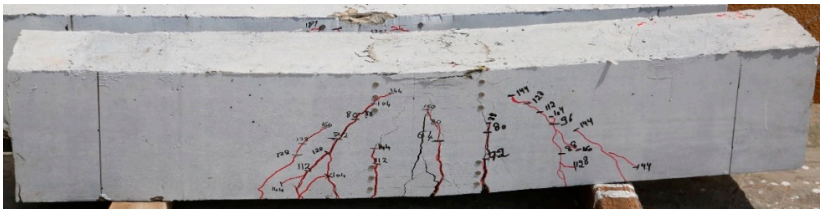

Figure 20. Crack pattern for beam PS-1.5.

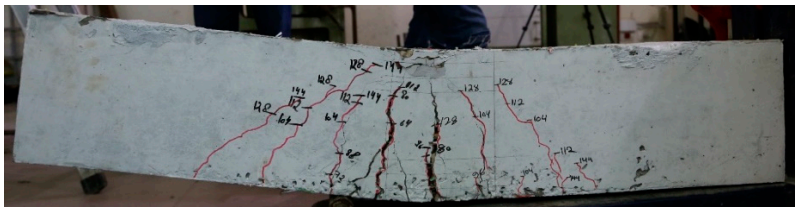

Figure 21. Crack pattern for beam PS-3.

3.2. *Numerical Results*

Numerical analysis results showed that the model was successfully validated to match the experimental results. This is shown in Figure 22 where the load deflection curves for all beams are presented. Similar to the experimental results, the numerical analysis showed that beam PS-0.5 had the highest load capacity with a load of 183 kN. Additionally, beam PS-3.0 had a maximum deflection of 41 mm compared with 16 mm for the control beam (PS-0) indicating higher ductility in the presence of 3% WPS. Table 6 summarizes the load capacity and maximum deflection results where the error between experimental and numerical values ranged between 3% and 10%.

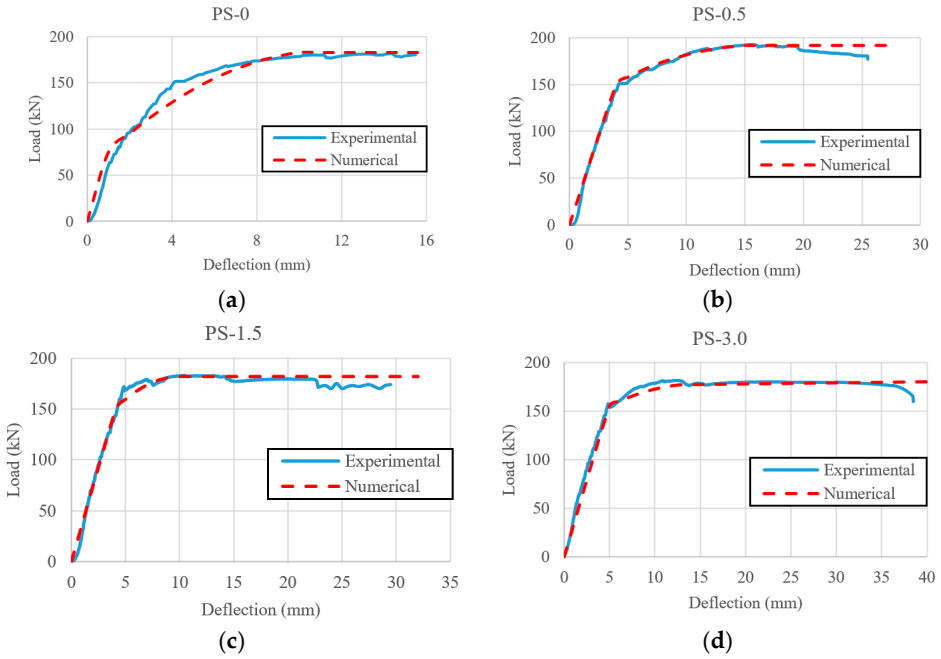

Figure 22. Experimental vs. numerical load–deflection curves for: (**a**) PS-0, (**b**) PS-0.5, (**c**) PS-1.5 and (**d**) PS-3.0.

Table 6. Experimental vs. numerical results.

Beam	Experimental		Numerical	
	Maximum Load "P_{max}" (kN)	Maximum Deflection Δ_u (mm)	Maximum Load "P_{max}" (kN)	Maximum Deflection Δ_u (mm)
PS-0	181.4	15.5	183.0	16.0
PS-0.5	192.7	25.5	192.0	27.0
PS-1.5	182.7	29.0	182.0	32.0
PS-3.0	181.3	38.4	180.0	41.0

Moreover, the damage pattern for all beams is presented below in Figure 23. These patterns were similar to the experimental ones, where beams with WPS fibers showed more cracks than the control beam (PS-0), which is due to the higher ductility for these beams compared to the control beam.

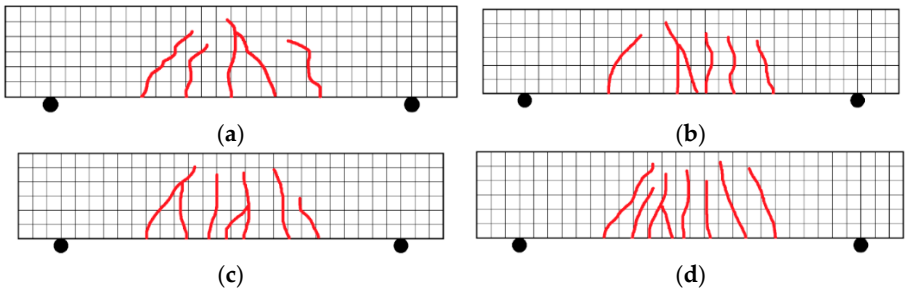

Figure 23. Numerical crack pattern for: (**a**) PS-0, (**b**) PS-0.5, (**c**) PS-1.5 and (**d**) PS-3.0.

4. Conclusions

The following conclusions were based on the findings of this study:

1. Adding 0.5% WPS fibers (by volume) resulted in a slight increase (3.4%) in concrete compressive strength. There was a decrease in compressive strength by 5.7% and 7.2% for concrete containing 1.5% and 3% WPS fibers respectively.
2. Adding WPS fibers showed an increase in the split tensile strength of concrete. As the percentage of WPS increased, the split tensile strength of concrete increased. The increasing percentages were 2.2%, 3.3% and 6.7% for specimens PS-0.5, PS-1.5 and PS-3 respectively. There was a slight increase in the ratio of split tensile to compressive strength from 10.8% for control specimen (PS-0) to 12.5% for specimen PS-3.
3. The load deflection curves showed a better ductility as the percentage of WPS fiber increased from 0 to 3%. The ductility factor ranged from 3.7 for the control beam (PS-0) to 8 for beams containing 3% WPS fiber (PS-3). The percentage increase in ductility was 65%, 70% and 116% for beams PS-0.5, PS-1.5 and PS-3 respectively. As for the maximum load capacity, all beams had nearly the same load regardless of the amount of WPS fiber.
4. The higher the percentage of WPS fibers in concrete, the higher the tensile strain at the same loading level. The tensile strain was 0.0012, 0.0016, 0.0019 and 0.0024 for beams PS-0, PS-0.5, PS-1.5 and PS-3 respectively. This is an increase of 100% in the presence of 3% WPS fiber. Additionally, the neutral axis depth was shifted to the top face as the load increased for all beams.
5. The load–defection curves derived from the numerical analysis seemed to be similar to those of the experimental curves. The error percentages for both maximum load capacity and maximum deflection ranged from 3% to 10%. This indicates that the parameters used in numerical modeling were suitable for predicting the load deflection curve and failure mode.
6. As a general conclusion, using 3% WPS fibers (by volume) results in an adequate strength and higher ductility compared with the control.

Author Contributions: J.M.K. and A.E. had the original idea for the study, A.J. was responsible for data collection and analysis, A.J. and J.M.K. drafted the manuscript, and A.E., H.A. and M.S. reviewed it. All authors have read and agreed to the published version of the manuscript.

Funding: This research received no external funding.

Conflicts of Interest: The authors declare no conflict of interest.

References

1. Guo, Y.-C.; Zhang, J.-H.; Chen, G.-M.; Xie, Z.-H. Compressive behaviour of concrete structures incorporating recycled concrete aggregates, rubber crumb and reinforced with steel fibre, subjected to elevated temperatures. *J. Clean. Prod.* **2014**, *72*, 193–203. [CrossRef]
2. Su, H.; Yang, J.; Ling, T.-C.; Ghataora, G.S.; Dirar, S. Properties of concrete prepared with waste tyre rubber particles of uniform and varying sizes. *J. Clean. Prod.* **2015**, *91*, 288–296. [CrossRef]
3. Hossain, F.Z.; Shahjalal, M.; Islam, K.; Tiznobaik, M.; Alam, M.S. Mechanical properties of recycled aggregate concrete containing crumb rubber and polypropylene fiber. *Constr. Build. Mater.* **2019**, *225*, 983–996. [CrossRef]
4. Bravo, M.; De Brito, J. Concrete made with used tyre aggregate: Durability-related performance. *J. Clean. Prod.* **2012**, *25*, 42–50. [CrossRef]
5. Khatib, J.; Jahami, A.; Elkordi, A.; Baalbaki, O. Structural performance of reinforced concrete beams containing plastic waste caps. *Mag. Civ. Eng.* **2019**, *91*, 73–79. [CrossRef]
6. Jahami, A.; Khatib, J.; Baalbaki, O.; Sonebi, M. Prediction of Deflection in Reinforced Concrete Beams Containing Plastic Waste. *SSRN Electron. J.* **2019**, 551–555. [CrossRef]
7. Khatib, J.; Jahami, A.; Baalbaki, O. Flexural characteristics of reinforced concrete beams containing lightweight aggregate in the tensile zone. In Proceedings of the Fifth International Conference on Sustainable Construction Materials and Technologies, Kingston University, London, UK, 14–17 July 2019; ISSN 2515-3048 (Print); ISSN 2515-3056 (Online).

8. Jahami, A.; Khatib, J.; Firat, S. Load deflection characteristics of reinforced concrete beams incorporating fibers made of waste plastic straw. In Proceedings of the 2nd International Turkish World Engineering and Science Congress, Antalya, Turkey, 7–10 November 2019; pp. 326–333.
9. Balaguru, P.N.; Shah, S.P. *Fibre Reinforced Cement Composites*; McGraw-Hill: New York, NY, USA, 1992; Chapter 13; p. 351.
10. Maniac, B. Experimental study & strength of concrete by using steel & glass fibers. *IRJET* **2016**, *3*, 261–267.
11. Fard, A.T.; Soheili, H.; Movafagh, S.R.; Ahmadi, P.F. Combined Effect of glass fiber and polypropylene fiber on mechanical property of self-compacting concrete. *Mag. Civ. Eng.* **2016**, *62*, 26–31. [CrossRef]
12. Vairagade, S.V.; Kene, K.S. Introduction to Steel Fiber Reinforced Concrete on Engineering Performance of Concrete. *Int. J. Sci. Technol. Res.* **2012**, *1*, 141.
13. Yakhlaf, M.; Safiuddin, M.; Soudki, K. Properties of freshly mixed carbon fibre reinforced self-consolidating concrete. *Constr. Build. Mater.* **2013**, *46*, 224–231. [CrossRef]
14. Donnini, J.; Bellezze, T.; Corinaldesi, V. Mechanical, electrical and self-sensing properties of cementitious mortars containing short carbon fibers. *J. Build. Eng.* **2018**, *20*, 8–14. [CrossRef]
15. Samani, M.A.; Lak, S.J. Experimental investigation on the mechanical properties of recycled aggregate concrete reinforced by waste carbon fibers. *Int. J. Environ. Sci. Technol.* **2018**, *16*, 4519–4530. [CrossRef]
16. Phong, N.T.; Fujii, T.; Chuong, B.; Okubo, K. Study on How to Effectively Extract Bamboo Fibers from Raw Bamboo and Wastewater Treatment. *J. Mater. Sci. Res.* **2011**, *1*. [CrossRef]
17. Kim, S.B.; Yi, N.H.; Kim, H.Y.; Kim, J.-H.J.; Song, Y.-C. Material and structural performance evaluation of recycled PET fiber reinforced concrete. *Cem. Concr. Compos.* **2010**, *32*, 232–240. [CrossRef]
18. Foti, D. Use of recycled waste pet bottles fibers for the reinforcement of concrete. *Compos. Struct.* **2013**, *96*, 396–404. [CrossRef]
19. Foti, D. *Recycled Waste PET for Sustainable Fiber-Reinforced Concrete*; Elsevier Ltd.: Amsterdam, The Netherlands, 2019.
20. Foti, D. Preliminary analysis of concrete reinforced with waste bottles PET fibers. *Constr. Build. Mater.* **2011**, *25*, 1906–1915. [CrossRef]
21. Wang, J.; Dai, Q.; Si, R.; Guo, S. Mechanical, durability, and microstructural properties of macro synthetic polypropylene (PP) fiber-reinforced rubber concrete. *J. Clean. Prod.* **2019**, *234*, 1351–1364. [CrossRef]
22. Sadrinejad, I.; Madandoust, R.; Ranjbar, M.M. The mechanical and durability properties of concrete containing hybrid synthetic fibers. *Constr. Build. Mater.* **2018**, *178*, 72–82. [CrossRef]
23. Khalid, F.; Irwan, J.; Ibrahim, M.W.; Othman, N.; Shahidan, S. Splitting tensile and pullout behavior of synthetic wastes as fiber-reinforced concrete. *Constr. Build. Mater.* **2018**, *171*, 54–64. [CrossRef]
24. Jahami, A.; Temsah, Y.; Khatib, J. The efficiency of using CFRP as a strengthening technique for reinforced concrete beams subjected to blast loading. *Int. J. Adv. Struct. Eng.* **2019**, *11*, 411–420. [CrossRef]
25. Temsah, Y.; Jahami, A.; Khatib, J.M.; Sonebi, M. Numerical Derivation of Iso-Damaged Curve for a Reinforced Concrete Beam Subjected to Blast Loading. *MATEC Web Conf.* **2018**, *149*, 1–5. [CrossRef]
26. Jahami, A.; Temsah, Y.; Khatib, J.; Baalbaki, O.; Darwiche, M.; Chaaban, S. Impact behavior of rehabilitated post-tensioned slabs previously damaged by impact loading. *Mag. Civ. Eng.* **2020**, *93*, 134–146. [CrossRef]
27. Temsah, Y.; Jahami, A.; Khatib, J.M.; Sonebi, M. Numerical analysis of a reinforced concrete beam under blast loading. *MATEC Web Conf.* **2018**, *149*, 02063. [CrossRef]
28. Temsah, Y.; Jahami, A.; Khatib, J.; Firat, S. Numerical study for RC beams subjected to blast waves. In Proceedings of the 1st International Turkish World Engineering and Science Congress in Antalya, Antalya, Turkey, 7–10 December 2017.
29. Temsah, Y.; Jahami, A.; Khatib, J.; Firat, S. Single degree of freedom approach of a reinforced concrete beam subjected to blast loading. In Proceedings of the 1st International Turkish World Engineering and Science Congress in Antalya, Antalya, Turkey, 7–10 December 2017.
30. ASTM C192/C192M—19 Standard Practice for Making and Curing Concrete Test Specimens in the Laboratory. Available online: https://www.astm.org/Standards/C192 (accessed on 31 March 2020).
31. BS EN 934-2: Admixtures for Concrete, Mortar and Grout Part 2: Concrete Admixtures—Definitions, Requirements, Conformity, Marking and Labelling. Available online: https://global.ihs.com/doc_detail.cfm?document_name=BSEN934-2&item_s_key=00290909 (accessed on 31 March 2020).
32. Khatib, J.; Jahami, A.; Baalbaki, O.; Elkordi, A.; Bakri, A.; Alaina, R. Performance of Concrete Containing Waste Plastic Straw Fibers. *BAU J. Sci. Technol.* **2020**, *1*, 1–10.

33. ASTM C39/C39M—20 Standard Test Method for Compressive Strength of Cylindrical Concrete Specimens. Available online: https://www.astm.org/Standards/C39 (accessed on 27 March 2020).
34. American Society for Testing and Materials. *ASTM C496/C496M-17, Standard Test Method for Splitting Tensile Strength of Cylindrical Concrete Specimens*; ASTM International: West Conshohocken, PA, USA, 2017; p. 5.
35. *ASTM D790-03, Standard Test Methods for Flexural Properties of Unreinforced and Reinforced Plastics and Electrical Insulating Materials*; ASTM International: West Conshohocken, PA, USA, 2003. Available online: www.astm.org (accessed on 9 December 2019).
36. *ASTM C78/C78M-18, Standard Test Method for Flexural Strength of Concrete (Using Simple Beam with Third-Point Loading)*; ASTM International: West Conshohocken, PA, USA, 2018. Available online: www.astm.org (accessed on 9 December 2019).
37. *ASTM C1609/C1609M-19, Standard Test Method for Flexural Performance of Fiber-Reinforced Concrete (Using Beam with Third-Point Loading)*; ASTM International: West Conshohocken, PA, USA, 2019. Available online: www.astm.org (accessed on 9 December 2019).
38. *ASTM E606/E606M-12, Standard Test Method for Strain-Controlled Fatigue Testing*; ASTM International: West Conshohocken, PA, USA, 2012. Available online: www.astm.org (accessed on 9 December 2019).
39. *ASTM E251-92(2014), Standard Test Methods for Performance Characteristics of Metallic Bonded Resistance Strain Gages*; ASTM International: West Conshohocken, PA, USA, 2014. Available online: www.astm.org (accessed on 9 December 2019).
40. ACI Committee. *Building Code Requirements for Structural Concrete (ACI 318-14)*; American Concrete Institute, ACI: Farmington Hills, MI, USA, 2014.